Published in final edited form as:
Magn Reson Med. 2013 February ; 69(2): 337–345. doi:10.1002/mrm.24254.

Simultaneous Non-contrast Angiography and intraPlaque hemorrhage (SNAP) imaging for carotid atherosclerotic disease evaluation

Jinnan Wang[1], **Peter Börnert**[2], **Huilin Zhao**[3], **Daniel S. Hippe**[4], **Xihai Zhao**[5], **Niranjan Balu**[4], **Marina S. Ferguson**[4], **Thomas S. Hatsukami**[6], **Jianrong Xu**[3], **Chun Yuan**[4,5], and **William S. Kerwin**[4]

[1]Clinical Sites Research Program, Philips Research North America, Briarcliff Manor, NY 10510

[2]Philips Research Europe, Hamburg, Germany

[3]Renji Hospital, Shanghai Jiaotong University, Shanghai, China

[4]Department of Radiology, University of Washington, Seattle, WA

[5]Department of Biomedical Engineering, Tsinghua University, Beijing, China

[6]Department of Surgery, University of Washington, Seattle, WA

Abstract

A Simultaneous Non-contrast Angiography and intraPlaque hemorrhage (SNAP) MR imaging technique is proposed to detect both luminal stenosis and hemorrhage in atherosclerosis patients in a single scan. 13 patients with diagnosed carotid atherosclerotic plaque were recruited after informed consent. All scans were performed on a 3T MR imaging system with SNAP, 2D time-of-flight (TOF) and magnetization-prepared 3D rapid acquisition gradient echo (MP-RAGE) sequences. The SNAP sequence utilized a phase sensitive acquisition, and was designed to provide positive signals corresponding to intraplaque hemorrhage (IPH) and negative signals corresponding to lumen. SNAP images were compared to TOF images to evaluate lumen size measurements using linear mixed models and the intraclass correlation coefficient (ICC). IPH identification accuracy was evaluated by comparing to MP-RAGE images using Cohen's Kappa. Diagnostic quality SNAP images were generated from all subjects. Quantitatively, the lumen size measurements by SNAP were strongly correlated (ICC=0.96, $p<0.001$) with those measured by TOF. For IPH detection, strong agreement ($\kappa=0.82$, $p<0.001$) was also identified between SNAP and MP-RAGE images. In conclusion, a Simultaneous Non-contrast Angiography and intraPlaque hemorrhage (SNAP) imaging technique was proposed and shows great promise for imaging both lumen size and carotid intraplaque hemorrhage with a single scan.

Keywords

MR Angiography; Intraplaque Hemorrhage; SNAP; Vessel Wall

Introduction

Luminal stenosis remains the current clinical standard for evaluating stroke risk due to carotid disease (1). Although contrast-enhanced MR angiography (MRA) has been shown to

Corresponding Author: Jinnan Wang, Address: 815 Mercer ST Rm 124, Seattle, WA 98109, Tel: (206)897-1312, FAX: (206)616-9354, jinnan.wang@philips.com.

provide highly accurate stenosis measurements in carotid artery disease (2), the risk of triggering nephrogenic systemic fibrosis (3) in patients with impaired renal function limits the application of contrast-enhanced MRA in clinical environments. Additionally, the requirement of acquiring images within the first-pass timeframe also limits the spatial resolution and signal-to-noise ratio (SNR) that can be achieved by such techniques. To overcome these issues, there has been clinical interest in using non-contrast enhanced MRA techniques as alternative approaches for luminal stenosis measurements (4–7).

Intraplaque hemorrhage (IPH) identified in the atherosclerotic plaque is also strongly associated with increased risks of clinical events (8–10) as well as plaque progression (11–12). IPH has also been suggested to be a potentially important factor in surgical planning (13). A number of MR imaging techniques have been developed to detect IPH in atherosclerotic plaques (14–16). All take advantage of the short T1 relaxation times of IPH components, which lead to hyperintensities on T1-weighted images. Among the techniques compared in a recent study (17), the magnetization-prepared rapid acquisition gradient echo (MP-RAGE) technique was found to have the highest sensitivity and specificity (17).

Given the established clinical importance of stenosis and the emerging interests in detecting IPH in patients at high risk of developing stroke, an efficient means for the assessment of both stenosis and IPH is desirable. The current MRA techniques are not optimal approaches to effectively detect IPH because 1) they are specifically optimized to visualize flowing spins but not IPH, and 2) both MRA and IPH are expected to have bright signals, thus confounding each other's detection, particularly when the hemorrhage is juxtaluminal. As a consequence, IPH information must now be separately acquired, at the expense of extra scanning time and with additional challenges arising from the need for image registration. These added technical challenges are substantial impediments to the integration of IPH imaging with MRA for carotid atherosclerosis evaluations.

In this manuscript, we propose a Simultaneous Non-contrast Angiography and intraPlaque hemorrhage (SNAP) imaging technique that allows both MRA and IPH evaluations in the same acquisition. The SNAP technique is based on the previously reported Slab-selective Phase-sensitive Inversion-Recovery (SPI) sequence (18). Taking advantage of the phase-sensitive reconstruction (19) used in SPI, the SNAP sequence generates images with negative signal corresponding to MRA and positive signal corresponding to IPH. By displaying only the negative signals, a non-contrast MR angiogram is rendered with no contamination from background tissues. Alternatively, displaying only the positive signals yields a highly T1-weighted image suitable for IPH detection. To test this concept, we sought to evaluate the ability of SNAP to measure lumen size and detect IPH by comparing with previously established time of flight (TOF) and MP-RAGE techniques.

Methods

Pulse sequence and optimization

The pulse sequence of SNAP is shown in Fig. 1a – each arrow represents a gradient echo acquisition with flip angle (FA) of α or θ, respectively. θ pulses are usually small FA pulses used to acquire the reference image. The reference image can estimate the background phase for accurate phase sensitive reconstruction (19). 5° is the default value of θ on our scanner and the value used in this study. A linear k-space filling scheme was used so that the central α pulse of the pulse train corresponded to the inversion time (TI) when the center of k-space was acquired. Fig. 1b shows the optimal signal curves of IPH, vessel wall and blood throughout the IRTR.

Optimization of the timing parameters and α in the SNAP sequence required derivation of an expression for the magnetization of each component (IPH, wall and lumen) at TI. Assuming the magnetization of static tissue before each IR has already reached its steady state M_{ss}, the magnetization before the first α pulse will be,

$$M_z(T_{gap}^-)=M_0-(M_0+M_{ss})\exp(-T_{gap}/T_1) \quad (1)$$

Right before the j^{th} (j>1) α pulse, the signal will be,

$$M_z(j_\alpha^-)=M_z(T_{gap}^-)(E_1\cos\alpha)^{j-1}+M_0(1-E_1)\frac{1-(E_1\cos\alpha)^{j-1}}{1-E_1\cos\alpha} \quad (2)$$

Where the relaxation term E_1 is given by $E_1=exp(-TR/T_1)$. Assume that the $(N+1)^{th}$ RF pulse corresponds to the TI time, because the linear k-space filling scheme is used, there will be 2N+1 α pulses and 2N+1 θ reference pulses. The signal level before the first θ pulse will be,

$$M_z(PS^-)=M_0(1-E_g)+M_z((2N+2)_\alpha^-)E_g \quad (3)$$

Where PS indicates the time when the low flip angle pulse train starts. The corresponding relaxation can be given as: $E_g=exp(-(T_{ex}+T_{gap})/T_1)$. The signal before the j^{th} (j>1) θ pulse will be,

$$M_z(j_\theta^-)=M_z(PS^-)(E_1\cos\theta)^{j-1}+M_0(1-E_1)\frac{1-(E_1\cos\theta)^{j-1}}{1-E_1\cos\theta} \quad (4)$$

After all 2N+1 θ pulses are carried out and a T_{ex} delay time, the signal right before the next IR pulse would give the steady state magnetization M_{ss}, i.e.,

$$M_{ss}=M_0(1-E_e)+M_z((2N+2)_\theta^-)E_e \quad (5)$$

Where $E_e=exp(-T_{ex}/T_1)$. Combining Eq. [1–5], the value of M_{ss} can be obtained. From Eq. [2], at the selected inversion time (TI), the signal level for IPH, vessel wall and blood can be written as,

$$M_z(TI)=(M_z(T_{gap}^-)(E_1\cos\alpha)^N+M_0(1-E_1)\frac{1-(E_1\cos\alpha)^N}{1-E_1\cos\alpha})\exp(-TE/T_2^*) \quad (6)$$

After solving numerically the value of M_{ss} from Eq. [1–5] and plugging Eq. [1] into Eq. [6], the signal level of static tissue components, IPH and wall, can be computed. Since the imaging parameters were optimized to make sure only fresh blood is imaged, the blood signal can also be calculated using Eq. [6] by simply setting the $M_z = 1$ before each IR.

The aim of the optimization was to select proper TI and flip angle α to maximize IPH-wall and wall-lumen contrasts at the same time. The following equation was used as the aim of the optimization,

$$\xi = C_{IPH-wall} + C_{wall-lumen} \quad (7)$$

Where, $C_{IPH\text{-}wall}$ is the magnetization difference between IPH and wall at the time of TI and $C_{wall\text{-}lumen}$ is the difference between wall and lumen. To maximize ξ, TI values between 200–1000ms and FA between 5°-25° were attempted. The parameter combination with the maximum ξ was selected as the optimized parameter for the following experiments. Once the TI and IRTR were determined, the thickness of the IR slab was optimized using a previously proposed approach (18).

In the simulation programmed in Matlab (R2010a, Mathworks, Natick, MA), the T_1 relaxation times used for different tissues were: IPH 500ms (16), wall 1115ms (20) and blood 1550ms (20); the T_2^* values used were: IPH 15ms (21), wall 20ms (20) and blood 275ms. Based on the current hardware/software settings, the minimum TR/TE values that can be achieved on the scanner were 10/4.8ms, T_{gap} and T_{ex} were 20 and 5ms.

In Vivo MR scan

In this Institutional Review Board approved study, 13 patients with 16%–99% carotid artery stenosis diagnosed by duplex ultrasound (Male: 9, Female: 4) were recruited after informed consent. One subject also underwent endarterectomy operation after the MR imaging.

All MR scans were performed on the 3T whole body scanner (Philips Achieva, R2.6.1, the Netherlands) using an 8-channel carotid coil (22). Besides the SNAP technique, traditional 2D TOF and MP-RAGE images were also acquired. 2D TOF, rather than its 3D counterpart, was selected because of its smaller in-flow volume (single slice vs. whole volume), which makes the images less susceptible to flow artifacts. The imaging parameters of the MP-RAGE sequence were optimized for 3T, as previously reported (16); the optimal FA and TI values identified in the simulation were used. The detailed imaging parameters of all the sequences are listed in Table 1.

Once the images were acquired, the MP-RAGE images were zero-padded in the slice direction to achieve 1mm slice thickness; SNAP images with a natural $0.8\times0.8\times0.8mm^3$ resolution were also zero-padded in all three directions to achieve $0.4\times0.4\times0.4mm^3$ voxel size.

Post-processing

By sequence design, the luminal signal on SNAP presents as negative values and the IPH signal presents as strong positive values. The original contrast of the SNAP image with both positive and negative values is shown in Fig. 2a. To measure the luminal area on the SNAP images, all positive values were set to zero and the absolute values of the images were displayed to achieve a positive lumen contrast (Fig. 2b). To evaluate the IPH lesions on the SNAP images, all negative values were set to zero (Fig 2c). To jointly evaluate both risk factors, the negative and positive values were coded with different colors for better visualization (Fig. 2d).

3D Maximum Intensity Projection (MIP) images of the color-coded SNAP images (Fig. 2e) were created from multiple projection angles to facilitate a comprehensive identification and evaluation of lesions. As shown in Fig. 2e, the location of IPH can be easily identified on the color-coded 3D MIP image.

Histology

For the one subject who underwent endarterectomy, the carotid plaque was removed using a special technique which leaves the lumen surface intact. The specimen was: fixed in 10% neutral buffered formalin, decalcified, processed, and then embedded en bloc in paraffin. Sections were collected at 1.0 mm intervals throughout the length of the plaque. After routine H&E and special Mallory's trichrome staining for hemorrhage detection, histology sections were matched to MR images using the bifurcation and lumen morphology as landmarks.

Lesion detection accuracy evaluation

To facilitate evaluation of the luminal area measurement accuracy, MRA were created out of SNAP and reformatted to 2mm axial slices with the original in-plane resolution. During image review, the reformatted SNAP images were first matched with the TOF images using the carotid artery bifurcation as a reference. On images more distal to bifurcation, internal carotid arteries were evaluated. Then the lumen areas on all matched locations from both sequences were separately delineated by a reviewer blinded to the image type, on a slice-by-slice basis.

To compare slice-based IPH detection accuracy, only arteries with IPH identified on either of the sequences were included to avoid the inflation of detection accuracy by large numbers of IPH-negative slices. SNAP images were reformatted to 1mm thickness to match the MP-RAGE images. After registration, the existence of IPH was separately identified on both MP-RAGE and reformatted SNAP images on a slice-by-slice basis by a reviewer blinded to the image type.

Statistical Analysis

We accounted for the non-independence of slice-based measurements by using linear mixed models (LMM) (23). The agreement between the lumen size measurements derived from both MR techniques was summarized using the intraclass correlation coefficient (ICC), which was derived from LMM parameters (23). A 95% confidence interval was computed using the parametric bootstrap and the percentile method (24). In addition, the lumen measurements were compared and summarized numerically and graphically using the methods of Bland and Altman, although modified to utilize LMM parameters (23,25).

All LMMs included random intercepts for each subject and each artery within subject. Furthermore, since it was anticipated that the correlation between slices of the same artery would vary depending on the distance between slices, several autocorrelation structures were explored. Specifically, all four parameter autoregressive moving average (ARMA) correlation structures were examined and the best fit was selected using the AIC criterion (26). This selection was done separately for each model.

Using only the arteries where IPH was detected, Cohen's Kappa (κ) was used to summarize the slice-based agreement between SNAP and MP-RAGE for IPH detection. A 95% confidence interval for κ was computed using a non-parametric bootstrap which resampled arteries using the percentile method (17). A generalized linear mixed model (GLMM) with random intercepts per artery and per location within artery was utilized to test whether IPH was more likely to be detected using SNAP or TOF.

All statistical calculations were conducted using R 2.11.0 (R Development Core Team. R Foundation for Statistical Computing, Vienna, Austria). The NLME package was used for fitting and evaluating LMMs (Jose Pinheiro, Douglas Bates, Saikat DebRoy, Deepayan Sarkar and the R Core team (2009). nlme: Linear and Nonlinear Mixed Effects Models. R

package version 3.1-96.). The lme4 package was used for fitting the GLMM (Douglas Bates and Martin Maechler (2010). lme4: Linear mixed-effects models using S4 classes. R package version 0.999375-34.).

Results

Pulse sequence optimization and contrast

As shown in Fig. 3a, TI=500ms and FA=11o were found to provide the highest combined IPH and lumen contrast among all imaging parameters. These values were selected as the optimal values in the following scans. As detailed in panel (b), it can be seen that when the optimized values were used, lumen signal remains negative and IPH presents strong positive signal.

With the optimized TI of 500ms, IRTR becomes 1970ms. Knowing 95% of the patients with luminal stenosis have flow velocity between 16–45cm/s (27), using the criteria established before (18), the IR slab coverage was determined as 62cm.

With the optimized parameters, the theoretical values of both the IPH-wall and wall-lumen contrasts were improved by the optimized SNAP design. When compared to the previous SPI design, in terms of normalized magnetization (M_z/M_0), the IPH-wall contrast improved by 35% (from 0.176 to 0.237) and the wall-lumen contrast improved by 13% (from 0.177 to 0.200).

In vivo MR scan

In vivo scans for all 13 subjects confirmed the expected contrast relationships. Sharp and clear lumen delineation on bilateral carotid artery was consistently observed throughout the 160mm longitudinal coverage on all subjects. No major flow artifacts were observed. In all cases, the TOF depictions of the carotid lumen qualitatively corresponded with negative SNAP signals. High signal regions on MP-RAGE, indicative of IPH, corresponded to similarly high-signal regions on SNAP. Visually, SNAP was consistently found to provide higher contrast between IPH and wall when compared to the MP-RAGE images. Fig. 4 shows a typical example.

Fig. 5 shows the results obtained from the one patient who underwent carotid endarterectomy. The 3D MIP images of the negative-portion (MRA), positive-portion (IPH) and the color-coded joint display demonstrated excellent visualization of luminal boundaries and intraplaque hemorrhage. It is noteworthy that even small branches of the carotid artery, as well as high-risk features like ulceration and high-level stenosis were accurately displayed. The corresponding histology slices confirmed the IPH, stenosis and ulceration on matched Mallory’s trichrome histology slices (Fig. 5d).

Lumen measurement accuracy evaluation

For the MRA evaluation on all 26 arteries imaged, 10 slices above and below the bifurcation including the slice on the bifurcation (21 slices in total) for each artery were included. Out of the total 546 locations, 43 were excluded due to insufficient coil sensitivity (32 locations) or insufficient coverage on TOF (11 locations).

Very good correlation was found between SNAP and TOF on lumen size measurements (ICC=0.96, 95% CI: 0.94–0.97), indicating a high level of consistency between the two techniques (Fig. 6). The average lumen size obtained from SNAP, however, was found to be larger than the one from TOF (SNAP: 32.3 ± 19.2 mm^2 vs. TOF 30.9 ± 17.7 mm^2).

IPH detection accuracy evaluation

At the artery level, a perfect correspondence between SNAP and MP-RAGE detection of IPH was observed. By both techniques, the same 8 arteries from 6 patients were identified as containing IPH and no IPH was detected in the remaining 18 arteries by either technique.

Out of the 8 arteries identified with IPH, the same slice coverage (10 slices above and below the bifurcation) for each artery was used. Of the total 168 locations, SNAP identified 68 of them as containing IPH, while MPRAGE identified 60, among which 57 agreed with SNAP. This corresponds to a Cohen's Kappa $\kappa = 0.82$ (95% CI: 0.67 – 0.94).

Discussion

The Simultaneous Non-contrast Angiography and intraPlaque hemorrhage (SNAP) imaging technique can detect both luminal stenosis and intraplaque hemorrhage with only a single scan. By using Phase-Sensitive reconstruction (19), the SNAP technique was optimized so that the luminal signal will always present as a negative signal while the IPH will always present as a strong positive signal. This approach offers a unique opportunity to detect two important risk factors of atherosclerosis disease within one scan but still maintains the flexibility to have them reviewed either individually or jointly. When jointly reviewed, MR angiography and IPH are always naturally registered so no extra registration approach will be needed. To facilitate the image review, they can also be color-coded to improve the visibility. As its detection accuracy has been demonstrated against established techniques, the SNAP technique has the potential to become the first-line imaging tool for patients at risk for stroke caused by atherosclerosis disease. It is important to realize that although the SNAP technique has been found to have good correspondence with the established imaging techniques, it still requires further comparison with histology and/or current clinical gold-standard to fully validate this technique.

In addition to the simultaneous detection of IPH, SNAP also presents other advantages compared to existing MRA techniques. SNAP already achieves resolution on par with latest CE-MRA techniques (28) without using parallel acquisition and could be further improved. Compared to the contrast-enhanced MRA technique, the SNAP technique does not require contrast injection and the acquisition time is not limited by the first-pass timeframe. Thus, SNAP imaging can be more flexibly designed for high-resolution acquisitions as it is less limited by time constraints compared to the traditional Gd enhanced scans. In addition, as most tissues present zero or negative signal on SNAP based MRA, SNAP images usually do not contain any unsuppressed background signal that is frequently observed on contrast-enhanced MRA images. This natural background suppression also helps to avoid the extra step of image subtraction as often needed for clinical contrast-enhanced MRA images (2).

When compared to in-flow based, non-contrast enhanced MRA techniques such as TOF, SNAP images are less susceptible to flow related artifacts. First, the period between two successive IR pulses, a period of 1.97 sec in this implementation, provides ample time for fresh blood infilling, including into regions of slow or circulating flow. Second, the use of a coronal imaging slab means that the blood signal is less likely to vary over the cardiac cycle due to pulsatile inflow of blood from outside of the slab. Third, the timing of the SNAP sequence has been optimized to maintain high contrast between the equilibrium magnetization and adjacent tissues. In combination, these factors ensure that the blood exhibits a comparatively homogeneous signal that is well differentiated from the background. In contrast, TOF techniques exhibit heterogeneous signals from fresh inflow as compared to slow or circulating flow. In addition, saturation of blood signal in slow flow regions leads to poor contrast with surrounding tissues. The benefits of SNAP may account for its apparent ability to visualize ulcers in the plaque surface. Ulcers are another high-risk

feature of atherosclerosis disease (29). Their detection can be challenging for non-contrast enhanced MRA techniques due to the complicated flow patterns around the ulceration.

The observation that SNAP maintains contrast for slow flowing blood may also account for the observation in this study that the lumen size by SNAP was slightly larger than by TOF. For a given TOF measurement, the corresponding SNAP measurement was on average 3.4% larger. As shown in the corresponding Bland-Altman plot (Fig. 7a), after removing the multiplicative bias, the limits of agreement were ± 10.4 mm^2. This is also exemplified by a sample image (Fig. 7b), where the lumen is not visible on TOF, but successfully identified by SNAP.

In terms of IPH detection, SNAP also provides higher IPH-wall contrast when compared to the existing IPH detection methods. As discussed in a previous study (18), the SPI technique can already provide significantly improved IPH contrast compared to MP-RAGE. Benefitting from the parameter optimization detailed in this manuscript, the SNAP technique can increase IPH-wall contrast by another 35%. With this improved contrast, the SNAP technique can potentially detect plaques with smaller or fragmented IPH lesions that would be otherwise overlooked by alternative techniques. In this study, SNAP identified more IPH lesions, although without reaching statistical significance (p=0.141). The increased detection of IPH is potentially due to the higher natural IPH-wall contrast provided by the SNAP technique. This finding is in agreement with the previous study comparing SPI and MP-RAGE (18). Although the SNAP technique was demonstrated on a 3T scanner in this study, it is expected to be applicable on a variety of MR imaging platforms, regardless of field strengths. It may require further optimization when first applied to different field strength due to the T1 relaxation time change.

The coronal SNAP acquisition allows for an approximately 3.5 times temporal efficiency improvements when compared to the original SPI technique. The extended coverage can improve the detection sensitivity of high risk lesions at the more proximal or distal locations that were otherwise not detectable at the outer limits. The isotropic resolution, on the other hand, can help eliminate inaccurate plaque burden measurements due to partial volume effects (30) and/or positioning error.

One challenge in achieving the gains in contrast and acquisition efficiency was how to balance the competing factors for optimization. The goals of the SNAP sequence include obtaining high contrast between IPH and wall, high contrast between wall and lumen, strong negative signals in the lumen, and strong positive signals in IPH. An objective function that simultaneously optimizes all of these factors is difficult to envision. We focused on optimizing contrast, with equal weighting of the different components. Alternative optimization schemes may be possible that yield better specific diagnostic capability with altered sequence timing.

With proper timing and flow optimization, the SNAP technique is also envisioned to be used to simultaneously detect stenosis and/or IPH in other vascular beds such as aortic or peripheral arteries. Compared to other clinically available non-contrast MRA techniques like Fresh Blood Imaging (31–32), the SNAP technique does not require a prep-scan and/or subtraction to generate MRA images in these vascular beds, although multiple SNAP acquisitions may be necessary to effectively image these arteries due to their larger extension and potentially slower blood flow. Furthermore, it may also be possible to adapt SNAP for other applications in which dual imaging would be beneficial. One potential application is to visualize the uptake of targeted contrast agents for molecular imaging. Tissues with T1-shortening contrast agent uptake would behave similarly to IPH and show

up as bright regions in the positive images, which could then be localized relative to the MRA.

One limitation of the SNAP technique is the visualization of both arterial and venous flow at the same time. Since the blood signal is inverted on a large region that is centered on the carotid bifurcation, flow from both directions is visualized on the SNAP image. On the other hand, testing results not presented here showed that non-inverted fresh blood appears bright at the upstream of the arteries. Therefore, should the inversion slab be placed to invert only the arterial flow, the spins from the non-inverted venous flow may present strong positive signal and confound the IPH detection. Besides, although SNAP is more robust to slow flow, its signal can still be susceptible to spin dephasing caused by turbulent flow. In theory, this is not expected to be more frequently observed on SNAP than on any other MR based imaging techniques, including contrast enhanced MRA. Still, we did observe some signal attenuation, although infrequently, on SNAP images acquired in this study. A larger study comparing SNAP with the clinical gold-standard is therefore important to better understand the frequency and impact of this artifact.

In conclusion, a Simultaneous Non-contrast Angiography and intraPlaque hemorrhage (SNAP) imaging technique was proposed and shows great promise for imaging both lumen size and carotid intraplaque hemorrhage with a single scan. With its large coverage, high resolution and simultaneous MRA/IPH images, SNAP has the potential to become the first-line imaging method for atherosclerosis patients in a clinical environment.

Acknowledgments

This study is partially funded by NIH grants 1R01HL103609 and 1R21NS072464.

References

1. Moore WS, Barnett HJ, Beebe HG, Bernstein EF, Brener BJ, Brott T, Caplan LR, Day A, Goldstone J, Hobson RW 2nd, Kempczinski RF, Matcher DB, Mayberg MR, Nicolaides AN, Norris JW, Ricotta JJ, Robertson JT, Rutherford RB, Thomas D, Toole JF, Trout HH 3rd, Wiebers DO. Guidelines for carotid endarterectomy. A multidisciplinary consensus statement from the ad hoc Committee. American Heart Association Stroke. 1995; 26(1):188–201.
2. Remonda L, Senn P, Barth A, Arnold M, Lovblad KO, Schroth G. Contrast-enhanced 3D MR angiography of the carotid artery: comparison with conventional digital subtraction angiography. AJNR Am J Neuroradiol. 2002; 23(2):213–219. [PubMed: 11847044]
3. Sadowski EA, Bennett LK, Chan MR, Wentland AL, Garrett AL, Garrett RW, Djamali A. Nephrogenic systemic fibrosis: risk factors and incidence estimation. Radiology. 2007; 243(1):148–157. [PubMed: 17267695]
4. Wedeen VJ, Meuli RA, Edelman RR, Geller SC, Frank LR, Brady TJ, Rosen BR. Projective imaging of pulsatile flow with magnetic resonance. Science. 1985; 230(4728):946–948. [PubMed: 4059917]
5. Brittain JH, Olcott EW, Szuba A, Gold GE, Wright GA, Irarrazaval P, Nishimura DG. Three-dimensional flow-independent peripheral angiography. Magn Reson Med. 1997; 38(3):343–354. [PubMed: 9339435]
6. Wang J, Yarnykh VL, Molitor JA, Nash RA, Chu B, Wilson GJ, Fleming J, Schwartz SM, Yuan C. Micro magnetic resonance angiography of the finger in systemic sclerosis. Rheumatology (Oxford). 2008; 47(8):1239–1243. [PubMed: 18559373]
7. Fan Z, Sheehan J, Bi X, Liu X, Carr J, Li D. 3D noncontrast MR angiography of the distal lower extremities using flow-sensitive dephasing (FSD)-prepared balanced SSFP. Magn Reson Med. 2009; 62(6):1523–1532. [PubMed: 19877278]
8. Singh N, Moody AR, Gladstone DJ, Leung G, Ravikumar R, Zhan J, Maggisano R. Moderate carotid artery stenosis: MR imaging-depicted intraplaque hemorrhage predicts risk of

cerebrovascular ischemic events in asymptomatic men. Radiology. 2009; 252(2):502–508. [PubMed: 19508983]

9. Altaf N, Daniels L, Morgan PS, Auer D, MacSweeney ST, Moody AR, Gladman JR. Detection of intraplaque hemorrhage by magnetic resonance imaging in symptomatic patients with mild to moderate carotid stenosis predicts recurrent neurological events. J Vasc Surg. 2008; 47(2):337–342. [PubMed: 18164171]
10. Takaya N, Yuan C, Chu B, Saam T, Underhill H, Cai J, Tran N, Polissar NL, Isaac C, Ferguson MS, Garden GA, Cramer SC, Maravilla KR, Hashimoto B, Hatsukami TS. Association between carotid plaque characteristics and subsequent ischemic cerebrovascular events: a prospective assessment with MRI--initial results. Stroke. 2006; 37(3):818–823. [PubMed: 16469957]
11. Underhill HR, Yuan C, Yarnykh VL, Chu B, Oikawa M, Polissar NL, Schwartz SM, Jarvik GP, Hatsukami TS. Arterial remodeling in the subclinical carotid artery disease. JACC Cardiovasc Imaging. 2009; 2(12):1381–1389. [PubMed: 20083072]
12. Takaya N, Yuan C, Chu B, Saam T, Polissar NL, Jarvik GP, Isaac C, McDonough J, Natiello C, Small R, Ferguson MS, Hatsukami TS. Presence of intraplaque hemorrhage stimulates progression of carotid atherosclerotic plaques: a high-resolution magnetic resonance imaging study. Circulation. 2005; 111(21):2768–2775. [PubMed: 15911695]
13. Hao H, Iihara K, Ishibashi-Ueda H, Saito F, Hirota S. Correlation of thin fibrous cap possessing adipophilin-positive macrophages and intraplaque hemorrhage with high clinical risk for carotid endarterectomy. J Neurosurg. 2011; 114(4):1080–1087. [PubMed: 20887090]
14. Moody AR, Murphy RE, Morgan PS, Martel AL, Delay GS, Allder S, MacSweeney ST, Tennant WG, Gladman J, Lowe J, Hunt BJ. Characterization of complicated carotid plaque with magnetic resonance direct thrombus imaging in patients with cerebral ischemia. Circulation. 2003; 107(24): 3047–3052. [PubMed: 12796133]
15. Chu B, Kampschulte A, Ferguson MS, Kerwin WS, Yarnykh VL, O'Brien KD, Polissar NL, Hatsukami TS, Yuan C. Hemorrhage in the atherosclerotic carotid plaque: a high-resolution MRI study. Stroke. 2004; 35(5):1079–1084. [PubMed: 15060318]
16. Zhu DC, Ferguson MS, DeMarco JK. An optimized 3D inversion recovery prepared fast spoiled gradient recalled sequence for carotid plaque hemorrhage imaging at 3. 0 T. Magn Reson Imaging. 2008; 26(10):1360–1366. [PubMed: 18583079]
17. Ota H, Yarnykh VL, Ferguson MS, Underhill HR, Demarco JK, Zhu DC, Oikawa M, Dong L, Zhao X, Collar A, Hatsukami TS, Yuan C. Carotid intraplaque hemorrhage imaging at 3. 0-T MR imaging: comparison of the diagnostic performance of three T1-weighted sequences. Radiology. 2010; 254(2):551–563. [PubMed: 20093526]
18. Wang J, Ferguson MS, Balu N, Yuan C, Hatsukami TS, Bornert P. Improved carotid intraplaque hemorrhage imaging using a slab-selective phase-sensitive inversion-recovery (SPI) sequence. Magn Reson Med. 2010; 64(5):1332–1340. [PubMed: 20597120]
19. Kellman P, Arai AE, McVeigh ER, Aletras AH. Phase-sensitive inversion recovery for detecting myocardial infarction using gadolinium-delayed hyperenhancement. Magn Reson Med. 2002; 47(2):372–383. [PubMed: 11810682]
20. Noeske R, Seifert F, Rhein KH, Rinneberg H. Human cardiac imaging at 3 T using phased array coils. Magn Reson Med. 2000; 44(6):978–982. [PubMed: 11108638]
21. Zhu DC, Vu AT, Ota H, DeMarco JK. An optimized 3D spoiled gradient recalled echo pulse sequence for hemorrhage assessment using inversion recovery and multiple echoes (3D SHINE) for carotid plaque imaging. Magn Reson Med. 2010; 64(5):1341–1351. [PubMed: 20574968]
22. Balu N, Yarnykh VL, Scholnick J, Chu B, Yuan C, Hayes C. Improvements in carotid plaque imaging using a new eight-element phased array coil at 3T. J Magn Reson Imaging. 2009; 30(5): 1209–1214. [PubMed: 19780187]
23. Diggle, P. Analysis of longitudinal data. Vol. xv. Oxford: Oxford University Press; 2002. p. 379
24. Davidson, AC.; Hinkley, DV. Bootstrap methods and their application. Cambridge University Press; 1997.
25. Bland JM, Altman DG. Measuring agreement in method comparison studies. Stat Methods Med Res. 1999; 8(2):135–160. [PubMed: 10501650]

26. Brockwell, PJ.; Davis, RA. Springer texts in Statistics. 2. 2002. Introduction to Time Series and Forecasting.
27. Mitrasinovic A, Radak S, Kolar J, Aleksic N, Otasevic P, Popovic M, Radak D. Color Doppler sonographic evaluation of flow volume of the internal carotid and vertebral arteries after carotid endarterectomy. J Clin Ultrasound. 2010; 38(5):238–243. [PubMed: 20127967]
28. Lohan DG, Tomasian A, Saleh RS, Singhal A, Krishnam MS, Finn JP. Ultra-low-dose, time-resolved contrast-enhanced magnetic resonance angiography of the carotid arteries at 3. 0 tesla. Invest Radiol. 2009; 44(4):207–217. [PubMed: 19300100]
29. Stone DA, Hawke MW, LaMonte M, Kittner SJ, Acosta J, Corretti M, Sample C, Price TR, Plotnick GD. Ulcerated atherosclerotic plaques in the thoracic aorta are associated with cryptogenic stroke: a multiplane transesophageal echocardiographic study. Am Heart J. 1995; 130(1):105–108. [PubMed: 7611098]
30. Antiga L, Wasserman BA, Steinman DA. On the overestimation of early wall thickening at the carotid bulb by black blood MRI, with implications for coronary and vulnerable plaque imaging. Magn Reson Med. 2008; 60(5):1020–1028. [PubMed: 18956420]
31. Miyazaki M, Sugiura S, Tateishi F, Wada H, Kassai Y, Abe H. Non-contrast-enhanced MR angiography using 3D ECG-synchronized half-Fourier fast spin echo. J Magn Reson Imaging. 2000; 12(5):776–783. [PubMed: 11050650]
32. Miyazaki M, Lee VS. Nonenhanced MR angiography. Radiology. 2008; 248(1):20–43. [PubMed: 18566168]

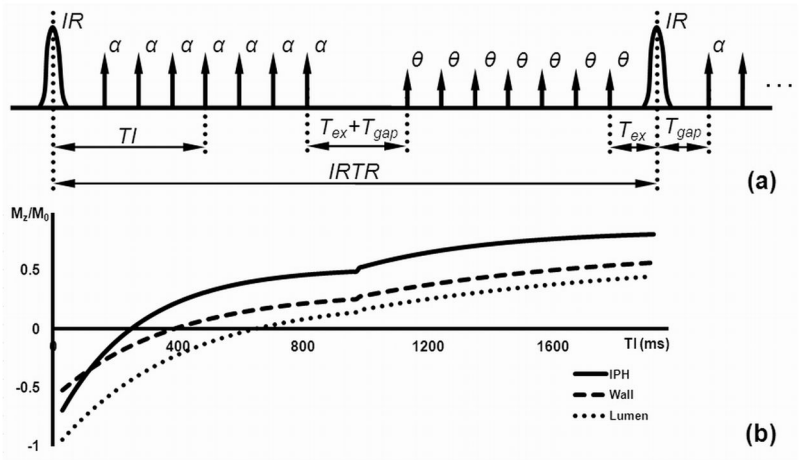

Figure 1.

(a)The pulse sequence of the SNAP sequence. The IR pulses are slab-selective with the slab perpendicular to the flow direction; each arrow between IR pulses represents a gradient-echo measured with a repetition time TR; α and θ are the flip angles for the image acquisition and phase corrections, respectively. TI is the delay between the IR pulse and the center of the gradient echo acquisition train; T_{gap} is the time gap between the IR pulse and the first gradient echo acquisition and T_{ex} is the time between the last gradient echo acquisition and the next IR. IRTR is the duration between the two consecutive IRs. For better visualization, T_{gap} and T_{ex} were not drawn proportionally. (b) The signal recovery curve of three main components (IPH, vessel wall, blood) in a whole IRTR. TI=500ms is the optimal value that provides the best contrast among the three.

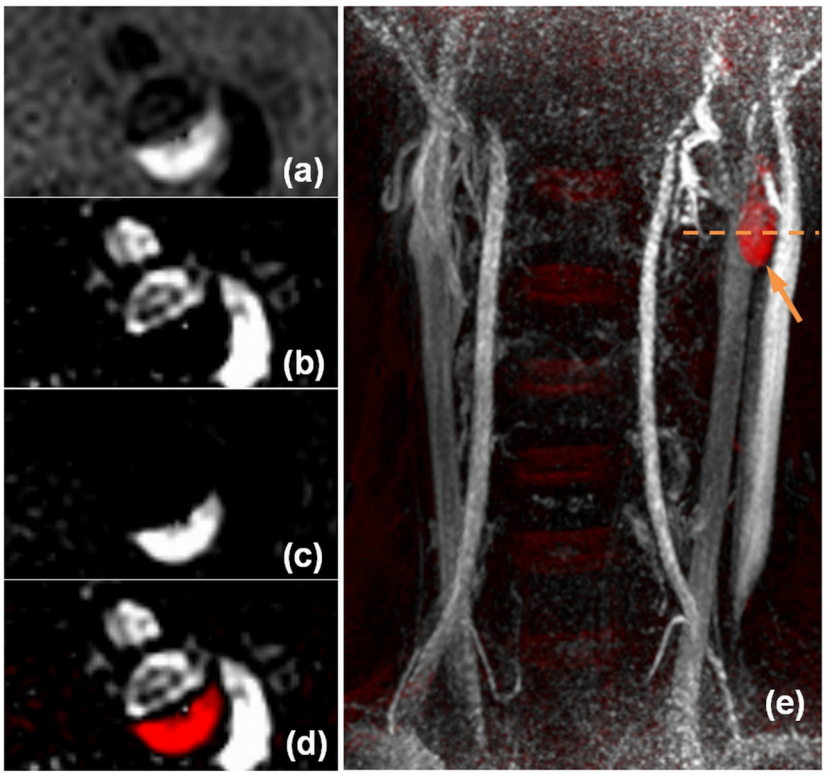

Figure 2.
Sample SNAP images and different viewing options. The original contrast of SNAP acquired cross-sectionally with both positive and negative values is shown in (a); the negative contrast (b) and positive contrast (c) SNAP images can be generated to evaluate lumen and IPH lesions. The color-coded SNAP image (d), which is by nature fully registered, can be used to jointly evaluate both risk factors. 3D MIP images (e) are also used to help facilitate the identification and evaluation of lesions. In this image, red-color labeled IPH lesion can be easily identified (arrow) and the dashed line indicates the location where images (a–d) were acquired. Notice the SNAP images (a–d) still represent good image quality although they were acquired at the peripheral region of the coil (notice the signal drop on e).

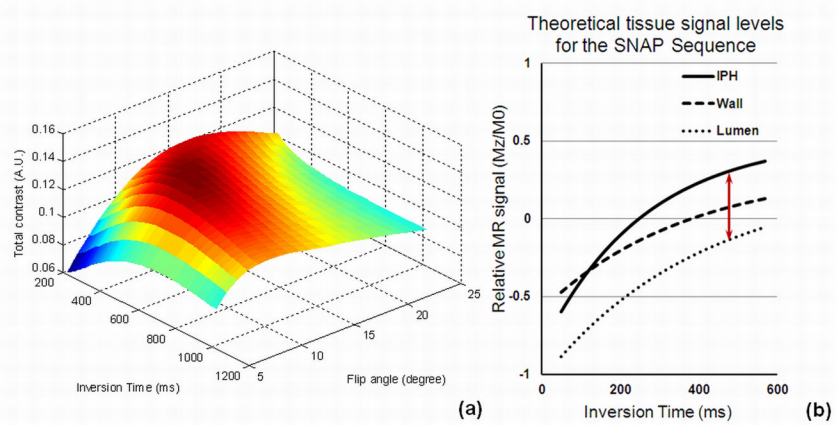

Figure 3.

SNAP sequence optimization. Panel (a) shows the optimization of TI and FA: the total contrast ξ maximized when TI=500ms and FA=11o. Panel (b) shows the theoretical signal curves of IPH wall and lumen at different TIs. As seen in this plot, when the optimal TI of 500ms (arrow) is used, the lumen signal remains negative while IPH presents a strong positive signal.

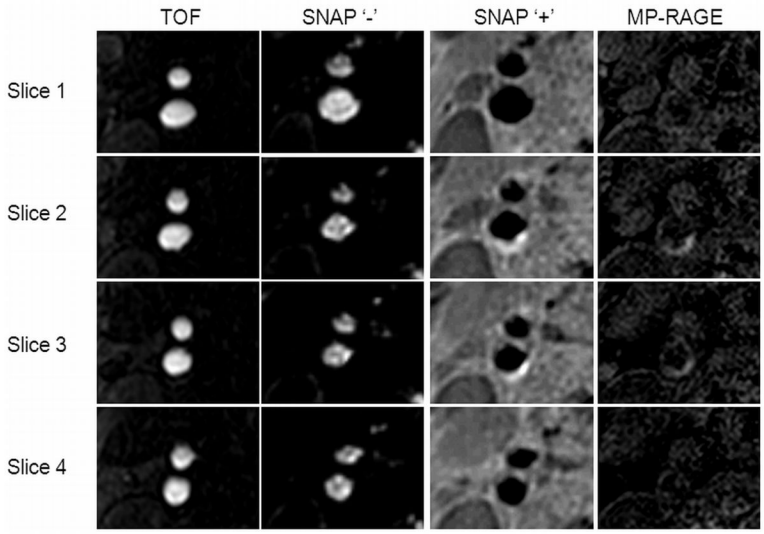

Figure 4.
SNAP comparison with TOF and MP-RAGE for lumen and IPH delineation. The negative portion of SNAP agrees well with TOF for lumen delineation while the positive portion of SNAP agrees well with MP-RAGE for IPH detection. SNAP was found to provide consistently higher IPH-wall contrast when compared to the MP-RAGE.

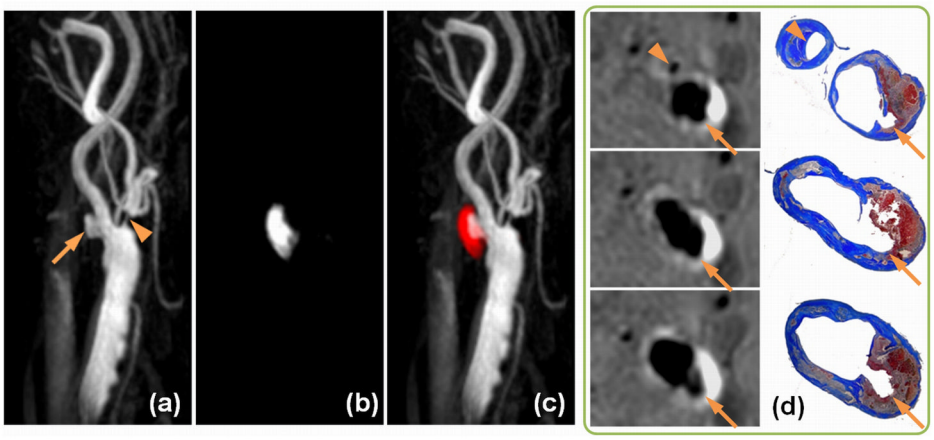

Figure 5.
SNAP with histology confirmation. 3D MIP images of the MRA-portion (a), IPH-portion (b) and color-coded joint view (c) of the SNAP images. Both IPH and luminal MRA were nicely delineated throughout the 160mm coverage of bilateral carotid arteries. Even small branches of the carotid artery, high-risk features like ulceration (Arrows) and high-level stenosis (Arrowheads) were visualized. On cross-sectional reformatted images (d), both IPH and luminal shapes were confirmed by the matched Mallory's trichrome histology slides.

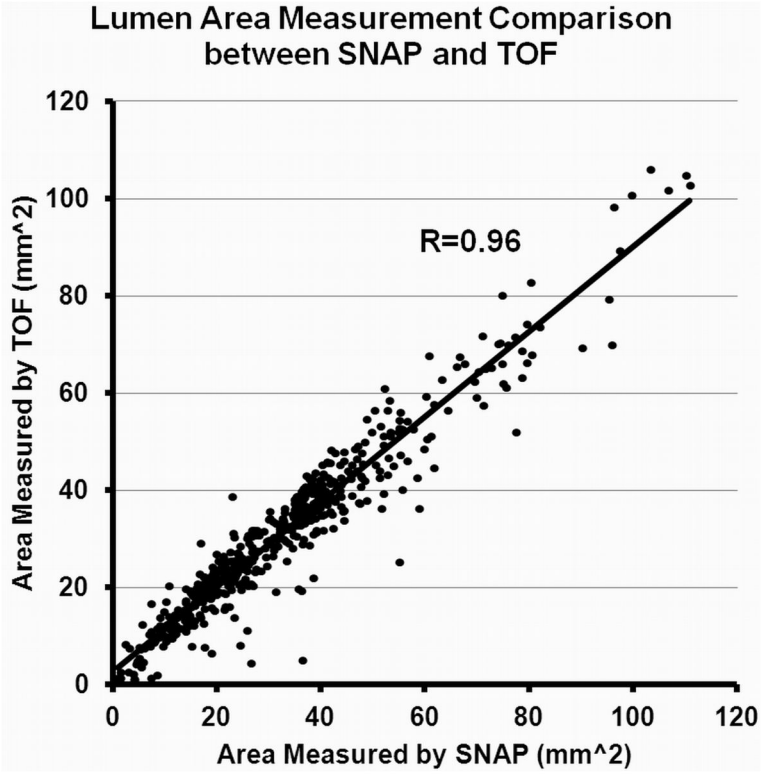

Figure 6.
Lumen size measurements comparison between SNAP and TOF. A very high agreement (ICC=0.96) between the two approaches were found.

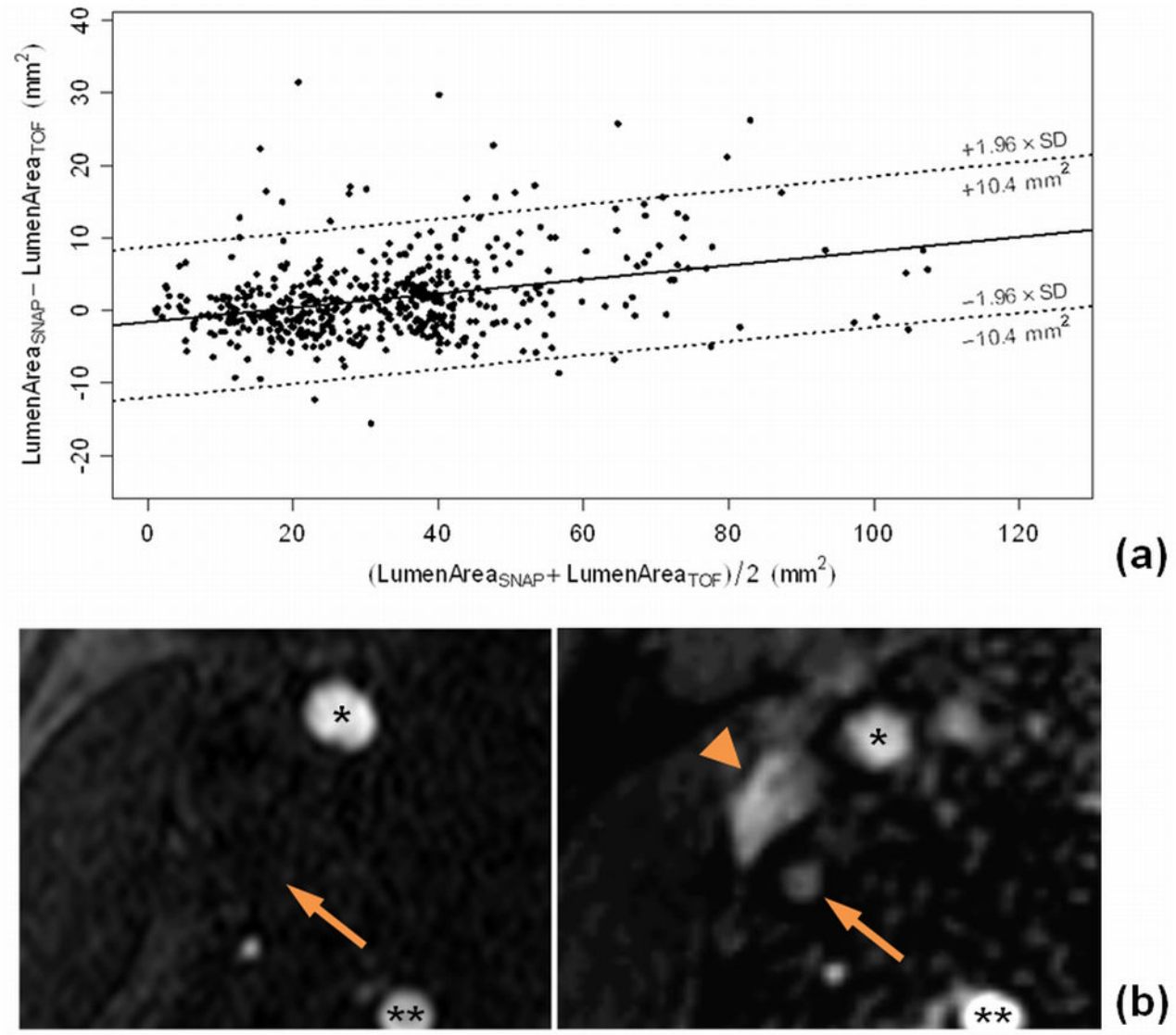

Figure 7.

(a) A Bland-Altman plot comparing lumen size measurements between SNAP and TOF revealed a bias between the two measurements and the dotted lines indicate the limits of agreement around the bias. SNAP was found to measure 3.4% larger lumen sizes than TOF. (b) Sample SNAP and TOF images demonstrated the relative underestimation of lumen size by TOF (left), compared to SNAP (right). As arrow indicated, the internal carotid artery is missing on the TOF image, but well delineated on SNAP image. The jugular vein (arrowhead) is also invisible on TOF due to venous flow saturation. *: External Carotid Arteries; **: Vertebral Arteries.

Table 1

In vivo imaging parameters of the sequences used

	Orientation	Dimension	TR (ms)	TE (ms)	FA(°)	TI (ms)	IRTR (ms)	FOV (mm)	Res (mm)	Thnk (mm)	PS*	FS**	NEX	Total Time
TOF	Axial	2D	14.5	4.0	40	N.A.	N.A.	160×120	0.63×0.63	2	N	N	1	1m40s
MP-RAGE	Axial	3D	13.2	3.2	15	304	568	160×160×32	0.6×0.6×2	N.A.	N	Y	1	1m16s
SNAP	Coronal	3D	10.0	4.8	11	500	1970	160×32×160	0.8×0.8×0.8	N.A.	Y	Y	2	5m17s

*: Phase Sensitive Reconstruction

**: Fat Suppression